10/5-19-97 JS (1)

SANDIA REPORT

SAND96-8614 • UC-1409
Unlimited Release
Printed June 1996

M97053036

Deposition Uniformity, Particle Nucleation and the Optimum Conditions for CVD in Multi-Wafer Furnaces

MASTER

DISTRIBUTION OF THIS DOCUMENT IS UNLIMITED

S. K. Griffiths, R. H. Nilson

Prepared by
Sandia National Laboratories
Albuquerque, New Mexico 87185 and Livermore, California 94550
for the United States Department of Energy
under Contract DE-AC04-94AL85000

Approved for public release, distribution is unlimited.

SF2900Q(8-81)

Issued by Sandia National Laboratories, operated for the United States Department of Energy by Sandia Corporation.
NOTICE: This report was prepared as an account of work sponsored by an agency of the United States Government. Neither the United States Government nor any agency thereof, nor any of their employees, nor any of the contractors, subcontractors, or their employees, makes any warranty, express or implied, or assumes any legal liability or responsibility for the accuracy, completeness, or usefulness of any information, apparatus, product, or process disclosed, or represents that its use would not infringe privately owned rights. Reference herein to any specific commercial product, process, or service by trade name, trademark, manufacturer, or otherwise, does not necessarily constitute or imply its endorsement, recommendation, or favoring by the United States Government, any agency thereof or any of their contractors or subconractors. The views and opinions expressed herein do not necessarily state or reflect those of the United States Government, any agency thereof or any of their contractors or subcontractors.

This report has been reproduced from the best available copy.

Available to DOE and DOE contractors from:

Office of Scientific and Technical Information
P.O. Box 62
Oak Ridge TN 37831

Prices available from (615) 576-8401, FTS 626-8401.

Available to the public from:

National Technical Information Service
U.S. Department of Commerce
5285 Port Royal Rd.
Springfield, VA 22161.

NTIS price codes
***Printed copy:* A02**
Microfiche copy: A01

DISCLAIMER

Portions of this document may be illegible electronic image products. Images are produced from the best available original document.

UC-1409

SAND96-8614
Unlimited Release
Printed June 1996

Deposition Uniformity, Particle Nucleation and the Optimum Conditions for CVD in Multi-Wafer Furnaces

Stewart K. Griffiths and Robert H. Nilson
Sandia National Laboratories
Livermore, California 94551-0969

A second-order perturbation solution describing the radial transport of a reactive species and concurrent deposition on wafer surfaces is derived for use in optimizing CVD process conditions. The result is applicable to a variety of deposition reactions and accounts for both diffusive and advective transport, as well as both ordinary and Knudsen diffusion. Based on the first-order approximation, the deposition rate is maximized subject to a constraint on the radial uniformity of the deposition rate. For a fixed reactant mole fraction, the optimum pressure and optimum temperature are obtained using the method of Lagrange multipliers. This yields a weak one-sided maximum; deposition rates fall as pressures are reduced but remain nearly constant at all pressures above the optimum value. The deposition rate is also maximized subject to dual constraints on the uniformity and particle nucleation rate. In this case, the optimum pressure, optimum temperature and optimum reactant fraction are similarly obtained, and the resulting maximum deposition rate is well defined. These results are also applicable to CVI processes used in composites manufacturing.

Introduction

Chemical vapor deposition (CVD) is widely used in microelectronics manufacturing to deposit thin layers of polycrystalline silicon, silicon dioxide and silicon nitride on single-crystal wafers [1,2]. These deposition processes employ a variety of chemistries and are usually performed in multi-wafer batch furnaces, each holding up to 300 wafers in a single stack. In order to maximize batch size and minimize stack height, the conventional inter-wafer space within the stack is typically just a few millimeters. Large batches tend to maximize furnace throughput because process cycle times are often dominated by the fixed overhead time associated with pushing and pulling the wafer boat, evacuating the furnace cavity, and ramping and stabilizing furnace temperatures. To further increase furnace throughput and to ensure high device yields, CVD process conditions for batch furnaces must be carefully optimized.

Although large batches and small inter-wafer spaces tend to maximize furnace throughput, they also tend to produce both axial and radial depletion of reactive gases and so give rise to nonuniformity of the deposition rate. Axial nonuniformity may be reduced by injecting gases at multiple points along the furnace length, decreasing the axial distance reactive species must be transported [3,4]. Although this complicates furnace design, there is no direct penalty in furnace throughput associated with multi-point injection. Similarly, the axial temperature profile in a batch furnace may be "tilted" such that axial depletion of reactive gases is just offset by increased temperatures so as to give little or no axial variation in the deposition rate [5]. In contrast, radial nonuniformity can be reduced by increasing the inter-wafer space [4,6], but this necessarily reduces the batch size and so may reduce furnace throughput. Alternatively, the processing conditions may be altered, as by reducing the pressure or temperature, to reduce radial nonuniformity [7,8]. This also reduces the deposition rate and so will also reduce furnace throughput. Because of these tradeoffs, any meaningful maximization of the deposition rate must be constrained by a requirement on the acceptable radial uniformity.

In addition to this concern about radial uniformity, deposition reactions can also lead to the gas-phase nucleation of particles [9,10]. Such particles may become embedded in the deposited layer and subsequently result in device failure. For this reason, reactant concentrations and other process conditions must be adjusted carefully to avoid excessive parti-

cle formation [11]. However, because those conditions giving low nucleation rates also yield low deposition rates, maximization of the deposition rate may also be constrained by an acceptable level of particle generation in the volume between wafer pairs.

Several other factors may also influence the optimum conditions for CVD processes. These include the morphology and electrical properties of the deposited layer [12], as well as conformity of the layer to device topography [13]. Here, however, we will address only the issues of deposition rate, radial deposition uniformity and particle nucleation.

Due to the complexity of problems involving coupled reaction and transport, most previous analyses of CVD have employed numerical methods. This approach permits detailed process simulations, including three-dimensional furnace geometries, spatially nonuniform temperatures, multi-point injection, and deposition mechanisms involving several to even dozens of reactive and product species [14,15,16]. However, while numerical methods are very powerful in treating complex problems in great detail, they are not particularly well suited to optimization due to relatively long execution times and to the very large number of solutions needed to optimize even two or three process conditions. In addition, constraints on the optimization pose a serious challenge for numerical methods since the process conditions satisfying those constraints are generally not known beforehand.

In this study we employ analytical methods to perform constrained maximizations of the deposition rate. This approach cannot address the detailed chemistry and complex geometry of numerical methods, but instead provides a more fundamental insight into the behavior of a somewhat simplified problem. Using a perturbation technique applicable to a range of deposition reactions, we first develop a fairly general relation between the deposition uniformity and process conditions. Based on this result, two distinct optimizations are then presented. In the first, the deposition rate is maximized subject to a single constraint on the radial deposition uniformity. In the second, the deposition rate is maximized subject to constraints on both radial uniformity and the gas-phase particle nucleation rate.

Governing Equations

To calculate radial nonuniformity in a wafer stack, we need only consider the region between any two adjacent wafers, as shown in Fig. 1. Even if axial depletion and axial nonuniformity are large, such a unit cell can adequately represent local conditions along the stack. Diffusive and advective transport in

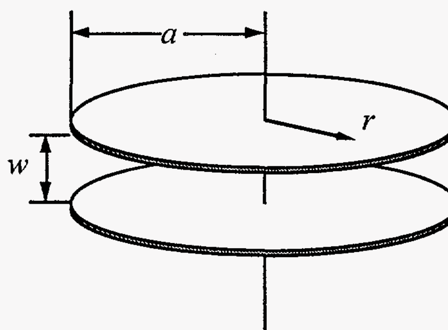

Figure 1. Schematic of a pair of wafers from the wafer stack. Reactive species are transported radially in the wafer gap by diffusion and advection. Depletion of reactants leads to a nonuniform deposition profile.

the space between these wafers and the accompanying reactant depletion due to deposition on wafer surfaces are described by continuity equations for each species, along with momentum and energy equations for the gas mixture. Here we consider one-dimensional transport in which species concentrations vary with radial position but are uniform in the axial direction across the inter-wafer space. Under this idealization, conservation of mass of a single reactive species may be written as

$$\frac{1}{r}\frac{d}{dr}\left(r\rho D\frac{df}{dr}\right) - \frac{1}{r}\frac{d}{dr}(r\rho u f) = 2\,\frac{S}{w} \qquad (1)$$

where r is the radial distance from the wafer center, ρ is the gas molar density, f is the reactive species mole fraction, D is the effective coefficient of binary diffusion for the reactive species, and u is the local molar-average fluid speed. The inter-wafer space, w, is the size of the open region between adjacent wafers. It is equivalent to the wafer pitch less the wafer thickness. Finally, S is the surface deposition rate; it may be any function of the pressure, temperature and reactant fraction. Note that the factor of two on the right of Eq. (1) accounts for surface reactions on both the front and back wafer faces.

Again assuming one-dimensional transport, continuity of the combined reactive and inert species can be expressed as

$$\frac{1}{r}\frac{d}{dr}(r\rho u) = 2\,\psi\,\frac{S}{w} \qquad (2)$$

where the parameter ψ is the net molar yield of gaseous products per mole of reactant; that is, the

molar ratio of gaseous products less reactants to reactants. By this definition, values of the parameter are limited to $\psi \geq -1$ since we are considering here only one reactive species. The limiting value of $\psi = -1$ corresponds to a simple single-species deposition reaction yielding solids but no gas-phase products.

The coefficient of diffusion in Eq. (1) must account for both ordinary and Knudsen diffusion. At high gas densities, collisions of the reactive species with gas molecules are much more common than are collisions with the wafer surfaces. In this limit, the diffusive flux of the reactive species is governed by ordinary diffusion. At sufficiently low pressures or sufficiently high temperatures, however, the mean free path of the reactive species becomes large relative to the size of the inter-wafer space. In this limit, collisions of the reactive species with wafer surfaces are predominant, and the diffusive flux is controlled by Knudsen diffusion. To account for both of these conditions, the overall effective coefficient of binary diffusion for the reactive species can be approximated by the Bonsanquet interpolation formula [17],

$$\frac{1}{D} = \frac{1}{D_m} + \frac{1}{D_{\mathrm{Kn}}} \tag{3}$$

where D_m denotes the effective binary coefficient of ordinary diffusion for the reactive species in the gas mixture, and D_{Kn} denotes the coefficient of Knudsen diffusion for the reactive species in the wafer space. Based on simple molecular theory [18], Eq. (3) may be rewritten as

$$D = \frac{\overline{v}\lambda}{3}\frac{\alpha w}{w + \alpha\lambda} = \frac{\overline{v}w}{3}\frac{\alpha \mathrm{Kn}}{1 + \alpha \mathrm{Kn}} \tag{4}$$

where $\mathrm{Kn} = \lambda/w$ is the Knudsen number based on properties of the reactive species and the size of the inter-wafer space, and $\overline{v}$ is the mean molecular speed of the reactive species.

$$\overline{v} = \left(\frac{8RT}{\pi m}\right)^{1/2} \tag{5}$$

Here R is the ideal gas constant, T is the gas temperature, and m is the reactive species molecular weight. The effective mean free path for the reactive species alone is given by

$$\lambda = \frac{RT}{\sqrt{2}\pi N \sigma^2 p} \tag{6}$$

where p is the total pressure, N is the Avogadro number, and σ is the molecular diameter of the reactive species.

The parameter α in Eq. (4) is the ratio of the effective binary coefficient of ordinary diffusion for the reactive species and the mixture of other furnace gases to the coefficient of ordinary self diffusion for the reactive species. As shown in Appendix A, this parameter depends only on the composition of the gas mixture and is independent of both the pressure and temperature for ideal gases. Thus for fixed gas composition, the parameter α is constant.

The continuity equations (1) and (2) must be accompanied by momentum and energy equations. In this analysis, we supplant the energy equations with an assumption that all gas species are at a uniform and constant temperature, T. Likewise, the momentum equation is replaced with an assumption that the pressure is uniform over the volume bounded by any two neighboring wafers. Based on results of the following analysis, it is fairly straightforward to show that this latter assumption remains valid whenever the deposition uniformity is high.

The governing transport equations are closed using an ideal gas equation of state, $p = \rho RT$. Because both the pressure and temperature are uniform and constant, this relation requires that the molar density is also uniform and constant.

To complete the mathematical statement of the transport and deposition problem, boundary conditions must be specified for the reactive species fraction and fluid speed. The second-order equation governing the reactive species requires two conditions. One is imposed by symmetry, requiring that the radial gradient of the reactive species vanish at the origin. For the second we assume that the reactive species mole fraction is fixed at the position of the wafer edge.

$$\frac{df}{dr} = 0 \text{ at } r = 0 \qquad f = f_a \text{ at } r = a \qquad (7a,b)$$

In addition, the first-order equation governing the fluid speed requires a single boundary condition. Again this is obtained from a symmetry condition at the position of the wafer center,

$$u = 0 \text{ at } r = 0 \tag{8}$$

requiring no flow into or out of the origin.

To normalize the governing equations, we introduce a dimensionless position, $x = r/a$, and two dimensionless dependent variables, $f^* = f/f_a$ and $u^* = ua/D$. Note that the normalized velocity u^* is equivalent to a local Peclet number, indicating the relative magnitudes of the advective and diffusive fluxes of the reactive species.

Applying these definitions to the transport equations yields the dimensionless governing equations

$$\frac{1}{x}\frac{d}{dx}\left(x\frac{df^*}{dx}\right) - \frac{1}{x}\frac{d}{dx}(x\,u^*f^*) + \frac{1}{D}\frac{\partial D}{\partial f^*}\left(\frac{df^*}{dx} - u^*f^*\right)\frac{df^*}{dx} = \beta \quad (9)$$

for the reactive species, and

$$\frac{1}{x}\frac{d}{dx}(x\,u^*) + \frac{u^*\partial D}{D\,\partial f^*}\frac{df^*}{dx} = \psi^*\beta \quad (10)$$

for total species conservation. The function β on the right of these equations is

$$\beta = \frac{2Sa^2}{\rho D w f_a} \quad (11)$$

and the new parameter appearing in Eq. (10) is the normalized reaction yield, $\psi^* = \psi f_a$. Boundary conditions for the normalized variables follow from Eqs. (7) and (8) in the obvious manner.

One additional relation can be obtained from Eqs. (1) and (2) by integrating each equation once and combining the two results. In the normalized form this yields

$$u^* = \frac{\psi^*}{1+\psi^* f^*}\frac{df^*}{dx} \quad (12)$$

giving the normalized fluid speed in terms of the normalized reactant mole fraction and its derivative alone. This relation applies everywhere and so is useful in separating the coupled reactive species and total conservation equations. Substituting Eq. (12) into Eq. (9) or (10) to eliminate u^* gives

$$\frac{1}{x}\frac{d}{dx}\left(\frac{x}{1+\psi^* f^*}\frac{df^*}{dx}\right) + \frac{1}{1+\psi^* f^*}\left(\frac{df^*}{dx}\right)^2\frac{1}{D}\frac{\partial D}{\partial f^*} = \beta \quad (13)$$

This species equation can now be solved without explicit knowledge of the local fluid speed. Fluid speeds can be computed after the fact from Eq. (12).

Equation (12) further provides useful insight into the relation between advective and diffusive fluxes of the reactive species. In dimensional form the advective flux at any position is $\rho u f$, while the magnitude of the diffusive flux is $\rho D\, df/dr$. The local ratio of advective to diffusive fluxes is therefore given by

$$\frac{\rho u f}{\rho D\, df/dr} = \frac{u^* f^*}{df^*/dx} = \frac{\psi^* f^*}{1+\psi^* f^*} \approx \frac{\psi^*}{1+\psi^*} \quad (14)$$

where the approximate equality on the right is due to the fact that $f^* \approx 1$ when the deposition rate is nearly uniform over the wafer surface. Taking into account the signs for each flux, we see that the total flux of the reactive species differs from the diffusive flux by a factor of $1/(1+\psi^* f^*)$. This is also apparent in Eq. (13), where this term serves as an apparent diffusivity in what otherwise appears as a simple diffusion-reaction equation. When ψ^* is positive, the total flux of the reactive species is therefore reduced by the flow of gas toward the wafer edge. When ψ^* is negative, the total flux is increased by flow toward the wafer center. Note that the total flux is quite sensitive to the deposition chemistry. For a net production of only one mole of gas per mole of reactant, $\psi = 1$, the advective transport reduces the net flux of reactive species toward the wafer center by up to a factor of two. This advective inhibition of diffusion in the inter-wafer space therefore may significantly reduce deposition uniformity when the reactant fraction is large.

Mathematical Method

High uniformity of deposited layers is almost always required in CVD wafer processing for microelectronics applications. We therefore seek perturbation solutions to the governing transport equations that are applicable only to this condition. Since the condition of high uniformity must correspond to a small value of the function β, we presume series solutions of the form

$$f^* = f_0^* + \beta_a f_1^* + \beta_a^2 f_2^* + \ldots \quad (15)$$

$$u^* = u_0^* + \beta_a u_1^* + \beta_a^2 u_2^* + \ldots \quad (16)$$

for the normalized reactant fraction and for the normalized fluid speed. The perturbation parameter is the function β evaluated at the conditions at the wafer edge.

$$\beta_a = \beta \quad \text{at} \quad f = f_a \quad (17)$$

The usual interpretation of the parameter β_a, referred to here as the surface deposition modulus, is that it is the square of the ratio of the characteristic time for diffusion to the characteristic time for surface deposition. In this view it is equivalent to the square of the Thiele modulus commonly appearing in analyses of porous-bed catalysis. Another useful interpretation of this parameter is that it is the ratio of two rates – the rate of deposition on both wafer surfaces, $2\pi a^2 S$, to the maximum rate of diffusive transport through the surface of a cylinder having a radius half that of the wafer and a height equal to the inter-wafer space,

$\pi w \rho D f_a$. Thus when β_a is small, the actual rate of diffusive transport will be less than this maximum, and the mean gradient of the reactant fraction will be smaller than the maximum value of f_a/a.

Because β on the right of Eqs. (9) and (10) is in general a function of the reactive species fraction, this must also be expanded in terms of the perturbation parameter. Expanding Eq. (11) about $f^* = f_0^*$ yields

$$\beta = \beta_a + (\mathbf{S}' - \mathbf{D}')\, f_1^* \beta_a^2 + O(\beta_a^3) \qquad (18)$$

where $\mathbf{S}'$ and $\mathbf{D}'$ are derivatives of the log of the deposition rate and diffusivity, taken at fixed pressure and temperature and evaluated at the condition $f^* = f_0^*$.

$$\mathbf{S}' = \frac{1}{S}\frac{\partial S}{\partial f^*} \quad \text{and} \quad \mathbf{D}' = \frac{1}{D}\frac{\partial D}{\partial f^*} \qquad (19a,b)$$

Note that the derivative of the log of the deposition rate is simply the order of the deposition reaction. Its value is unity for a irreversible first-order reaction, two for a second-order process, and the like. For more complex deposition reactions, having both forward and reverse rates or involving poisons, its value will generally depend on the pressure, temperature and reactive species fraction. The derivative of the diffusivity is, by analogy, the order of the diffusivity with respect to the reactant fraction. From Eq. (4) it is given by

$$\frac{1}{D}\frac{\partial D}{\partial f^*} = \frac{1}{1+\alpha \mathrm{Kn}}\;\frac{1}{\alpha}\frac{\partial \alpha}{\partial f^*} \qquad (20)$$

As discussed later, however, its value is near zero under a rather broad range of conditions.

To satisfy the normalized boundary conditions for all β_a and all ψ^*, the zeroth-order contributions to each series must satisfy $f_0^* = 1$ at $x = 1$, and $df_0^*/dx = 0$ and $u_0^* = 0$ at $x = 0$. All higher-order terms must satisfy

$$\frac{df_i^*}{dx} = 0 \;\text{ at }\; x = 0 \qquad f_i^* = 0 \;\text{ at }\; x = 1 \quad (21a,b)$$

$$u_i^* = 0 \;\text{ at }\; x = 0 \qquad (22)$$

for the reactive species fraction and fluid speed at the wafer edge or center.

By inspection of Eqs. (9) and (10), the zeroth-order solutions are $f_0^* = 1$ and $u_0^* = 0$. These of course are the trivial solutions for no surface deposition reaction, as appropriate for the limit $\beta_a \to 0$.

Substituting the zeroth-order solutions into Eqs. (9) and (10) and grouping like terms yields

$$\frac{1}{x}\frac{d}{dx}\left(x\frac{df_1^*}{dx}\right) = 1 + \psi^* \qquad (23)$$

$$\frac{1}{x}\frac{d}{dx}(x\, u_1^*) = \psi^* \qquad (24)$$

for the first-order terms. Integrating twice and applying the boundary conditions (21a,b) and (22) gives

$$f_1^* = \frac{1+\psi^*}{4}(x^2 - 1) \qquad u_1^* = \frac{\psi^*}{2}x \qquad (25a,b)$$

for the first-order normalized reactive species fraction and fluid speed. Note that the latter result can be obtained either from Eq. (12) or from integrating Eq. (24).

One interesting aspect of these first-order solutions is their dependence on the reaction chemistry. Both the parabolic profile of the reactant fraction and the linear profile of the fluid speed vary linearly with reaction yield, ψ^*. Because the first-order correction to the deposition rate will be proportional to the first-order reactive species concentration, the deposition uniformity will also vary linearly with reaction yield. In the limit $\psi^* \to -1$, however, the fluid speed becomes $u_1^* = -x/2$, indicating flow toward the wafer center. For this case, in which the gas is purely the reactive species and the deposition reaction yields no gas-phase products, the first-order fraction of the reactive species vanishes, $f_1^* = 0$, as does the first-order diffusive flux, df_1^*/dx. Species transport is due to advection only, and the deposition profile remains perfectly uniform even for finite deposition rates.

Governing equations for the second-order species fraction and fluid speed are obtained by substituting the first-order solutions into Eqs. (9) and (10) and collecting those non-zero terms containing the square of β_a. This gives

$$\frac{1}{x}\frac{d}{dx}\left(x\frac{df_2^*}{dx}\right) = \left(u_1^* - \mathbf{D}'\frac{df_1^*}{dx}\right)\frac{df_1^*}{dx} + \left[\psi^* + (1+\psi^*)(\mathbf{S}' - \mathbf{D}')\right] f_1^* \qquad (26)$$

for the reactant fraction, and

$$\frac{1}{x}\frac{d}{dx}(x\, u_2^*) = (\mathbf{S}' - \mathbf{D}')\psi^* f_1^* - u_1^* \mathbf{D}'\frac{df_1^*}{dx} \qquad (27)$$

for the fluid speed. Note again that the derivatives of the deposition rate and diffusivity are evaluated at the condition $f^* = f_0^* = 1$ and are therefore constants in these equations.

Integrating Eq. (26) twice and applying the appropriate boundary conditions yields

$$f_2^* = \frac{1+\psi^*}{64} \Big[\!\Big[\big[\psi^* - (1+\psi^*)\mathbf{D}'\big](x^4-1) + \big[\psi^* + (1+\psi^*)(\mathbf{S}'-\mathbf{D}')\big](x^4-4x^2+3) \Big]\!\Big] \quad (28)$$

for the normalized reactant fraction. Similarly, the second-order solution for the radial fluid speed obtained from Eq. (27) is

$$u_2^* = \frac{\psi^*}{16}(1+\psi^*)\left[\mathbf{S}'(x^3-2x) - 2\,\mathbf{D}'(x^3-x)\right] \quad (29)$$

Again these second-order terms satisfy Eq. (12) relating the fluid speed to the gradient of the reactive species mole fraction.

Deposition Uniformity

The deposition uniformity, U, is defined here as the ratio of the deposition rate at the wafer center to that at the wafer edge. Since the pressure and temperature do not vary with radial position, the variation in deposition rate depends only on the variation in reactant fraction. The deposition uniformity can therefore be obtained by expanding the deposition rate in a Taylor series about $f^* = 1$ and dividing the result by the rate at the wafer edge. This gives

$$U = 1 + \mathbf{S}'(\beta_a f_1^* + \beta_a^2 f_2^* + \ldots) + \frac{1}{2}\mathbf{S}''(\beta_a f_1^* + \ldots)^2 + \ldots \quad (30)$$

where the second derivative of the deposition rate with respect to the reactant fraction is

$$\mathbf{S}'' = \frac{1}{S}\frac{\partial^2 S}{\partial f^{*2}} \quad \text{at} \quad f^* = 1 \quad (31)$$

Combining these expressions with the reactant fraction perturbation solution and evaluating the result at $x = 0$, the uniformity may be written as

$$U = 1 - \frac{1+\psi^*}{4}\mathbf{S}'\beta_a + \frac{1+\psi^*}{64}\Big[\!\Big[\big[2\psi^* + (1+\psi^*)(3\,\mathbf{S}' - 2\,\mathbf{D}')\big]\mathbf{S}' + 2(1+\psi^*)\mathbf{S}''\Big]\!\Big]\beta_a^2 + O(\beta_a^3) \quad (32)$$

For the special case of a first-order deposition reaction, $\mathbf{S}' = 1$, and a diffusivity that is insensitive to the reactive species concentration, $\mathbf{D}' = 0$, Eq. (32) reduces to

$$U = 1 - \frac{1+\psi^*}{4}\beta_a + \frac{1+\psi^*}{64}(3+5\psi^*)\beta_a^2 + \ldots \quad (33)$$

Note that the uniformity, as defined here, approaches unity as the reaction rate falls to zero. In practice, however, uniformity is often described as the fractional deviation from a perfectly uniform condition. This alternative definition is actually that of a nonuniformity, given by the difference $1 - U$.

The expression obtained here for the deposition uniformity agrees to first order with a previous result for which the deposition reaction is a first-order process and advective fluxes are neglected [7]. The result in that analysis is $U = 1/(1+\beta_a/4)$. Expanding this expression for small β_a yields $U = 1 - \beta_a/4$, which is identical to the first-order term of Eq. (33) for the special case of $\psi^* = 0$. Recall that the condition $\psi^* = \psi f_a = 0$ corresponds to no net gain or loss of gas-phase species in the deposition process or to a process condition in which the reactant fraction is very small. In either case, no advective fluxes arise. Equations (25a) and (32) also agree to first order with previous analyses based on a collocation technique [8,19]. That analysis includes both advective and diffusive transport and is also applicable to a range of deposition reactions. In that case, however, the results are obtained in an implicit form typical of the collocation method.

Calculated uniformities are shown in Fig. 2 for the case of a first-order deposition reaction, $\mathbf{S}' = 1$, and no variation in the diffusivity with reactant fraction, $\mathbf{D}' = 0$. Solutions are plotted for a range of values of the normalized reaction yield, ψ^*. Both the first and second-order perturbation solutions are shown in this figure as solid curves. The dashed curves are numerical solutions to Eqs. (9) and (10). These numerical results were obtained by solving Eq. (13) directly using a very accurate shooting technique. They are presented here only to help evaluate the accuracy and valid range of the perturbation solutions.

Similarly, the normalized fluid speed at the wafer edge is shown in Fig. 3. Recall that the normalized speed is a local Peclet number. These results were obtained by evaluating Eqs. (25b) and (29) at $x = 1$ to yield

$$u_a^* = \frac{\psi^*}{2}\beta_a - \frac{\psi^*}{16}(1+\psi^*)\,\mathbf{S}'\beta_a^2 + O(\beta_a^3) \quad (34)$$

Note that fluid speeds at the perimeter and at the wafer center do not depend on the variation in diffusivity, but do exhibit such a dependence at intermediate positions along the wafer radius. Also note that

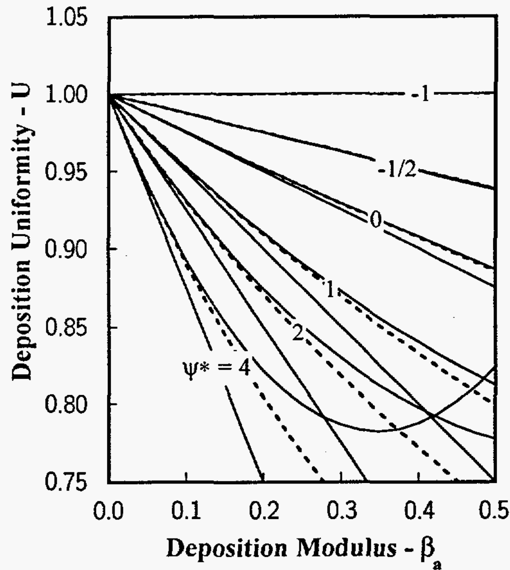

Figure 2. Deposition uniformity. Dashed curves represent numerical solutions to Eq. (13); solid curves are the one and two-term perturbation results. Increasing ψ^* reduces uniformity due to outward flow.

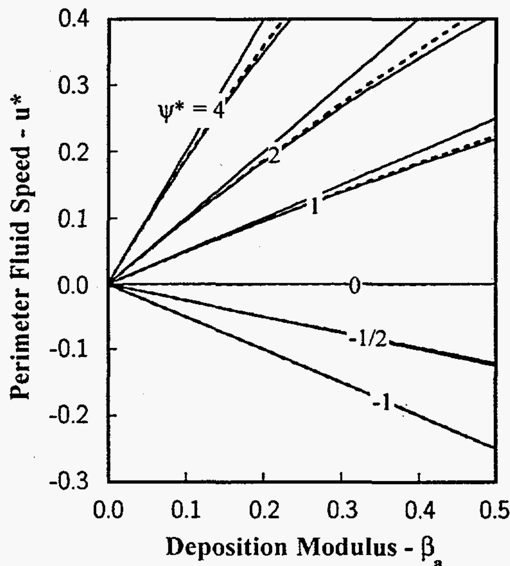

Figure 3. Normalized fluid speeds at wafer edge. Solid and dashed curves represent analytical and numerical results. Speeds increase with increasing ψ^* due to increased generation of product gases.

the first-order contribution to the fluid speed does not depend on the order of the deposition reaction.

Based on comparing the numerical and analytical results in Figs. 2 and 3, we find that the first-order correction to the deposition nonuniformity is accurate to within 14% for reaction yields in the range $-1 \leq \psi^* \leq 4$ and all uniformities greater than 0.9. The second-order perturbation solution for the deposition nonuniformity is accurate to about 2% for the same conditions. Similarly, the first-order fluid speed at the wafer edge is accurate to 6%, while the second-order solution is accurate to better than 1%.

Optimum Conditions At Fixed Uniformity

To identify optimum conditions for the CVD process we seek to maximize the deposition rate subject to the side condition of a minimum acceptable radial uniformity. In general, the deposition rate can always be increased by raising the pressure and temperature; thus, any unconstrained maximization of the deposition rate yields only the trivial solution of both pressure and temperature increasing without bound while the uniformity approaches zero. Because of this behavior, the constrained maximum deposition rate should occur when the uniformity constraint is just marginally satisfied. This permits replacing the inequality constraint of a minimum uniformity by an equality constraint that is satisfied exactly.

The constrained maximum deposition rate is defined by the requirement that the variation in rate with respect to all independent variables is zero along the direction of constant uniformity. To obtain this maximum we employ the method of Lagrange multipliers [20]. This technique introduces one new unknown constant for each constraint and yields one additional equation for each independent variable. The two new equations are

$$\frac{\partial S}{\partial p} - \kappa \frac{\partial U}{\partial p} = 0 \quad \text{and} \quad \frac{\partial S}{\partial T} - \kappa \frac{\partial U}{\partial T} = 0 \qquad (35a,b)$$

where κ, the Lagrange multiplier, is the new unknown constant. Together with the original constraint on the deposition uniformity, Eq. (32), this pair of equations can be solved for the optimum pressure and temperature yielding the maximum deposition rate.

Rearranging Eqs. (35a) and (35b) to eliminate κ yields

$$\frac{\partial S}{\partial p}\frac{\partial U}{\partial T} = \frac{\partial S}{\partial T}\frac{\partial U}{\partial p} \qquad (36)$$

Now using the first-order term from Eq. (32) describing the general form of the deposition uniformity, and

recalling from Eq. (11) that the deposition modulus depends on the pressure and temperature through the deposition rate, diffusivity and density, Eq. (36) may be rewritten in the form

$$\frac{1}{S}\frac{\partial S}{\partial p}\left(\frac{1}{\mathrm{S}'}\frac{\partial \mathrm{S}'}{\partial T}-\frac{1}{\rho}\frac{\partial \rho}{\partial T}-\frac{1}{D}\frac{\partial D}{\partial T}\right)= \frac{1}{S}\frac{\partial S}{\partial T}\left(\frac{1}{\mathrm{S}'}\frac{\partial \mathrm{S}'}{\partial p}-\frac{1}{\rho}\frac{\partial \rho}{\partial p}-\frac{1}{D}\frac{\partial D}{\partial p}\right) \quad (37)$$

Note that one product of derivatives of the deposition rate with respect to pressure and temperature has been canceled from each side of this expression.

The pair of equations (32) and (37) provide a fairly general statement of the conditions at which the deposition rate is maximum for a specified minimum uniformity. No assumptions regarding the form of the deposition reaction are required to obtain these expressions. The only required conditions are that transport within the inter-wafer space and deposition on wafer surfaces are adequately described by Eqs. (1) and (2) and that the radial nonuniformity of the deposition rate is small. Because of this generality, these equations can be used in simple numerical schemes to identify optimum processing conditions, even when the deposition reaction is a complex function of the pressure, temperature and reactant fraction.

Sample Calculations - Fixed Uniformity

Equation (37) above and the uniformity constraint can be solved in closed form for the optimum pressure and optimum temperature given a few simplifying assumptions. If the deposition process is a first order reaction having an Arrhenius temperature dependence, the surface reaction rate, S, can be expressed as the product of the surface impingement rate and a reaction probability, ϕ. In terms of the gas molecular density and reactant mole fraction, this is

$$S=\frac{\overline{v}}{4}\rho f\phi \quad \text{where} \quad \phi=b\,e^{-E_a/RT} \quad (38)$$

The mean molecular speed, $\overline{v}$, of the reactive species is given by Eq. (5). As before, ρ is the gas molar density, f is the reactive species mole fraction, R is the ideal gas constant, and T is the uniform gas temperature. The parameters b and E_a are the surface reaction pre-exponential constant and the apparent activation energy, respectively.

For such a deposition process, the order of the reaction is constant at $\mathrm{S}'=1$. From Eq. (4) describing the diffusivity based on simple kinetic theory and the ideal gas equation of state, Eq. (37) can then be written as

$$\frac{1}{S}\frac{\partial S}{\partial p}\left(\frac{1}{1+\alpha\mathrm{Kn}}-\frac{1}{2}\right)\frac{p}{T}=\frac{1}{S}\frac{\partial S}{\partial T}\left(\frac{\alpha\mathrm{Kn}}{1+\alpha\mathrm{Kn}}\right) \quad (39)$$

Now using Eq. (38) to evaluate the derivatives of the deposition rate with respect to the pressure and temperature gives

$$\frac{1}{S}\frac{\partial S}{\partial p}=\frac{1}{p} \qquad \frac{1}{S}\frac{\partial S}{\partial T}=\frac{1}{T}\left(\frac{E_a}{RT}-\frac{1}{2}\right) \quad (40a,b)$$

Substituting these expressions into Eq. (39) yields one of the two equations for the optimum conditions in terms of the pressure and temperature alone.

$$\frac{1}{1+\alpha\mathrm{Kn}}-\frac{1}{2}=\left(\frac{E_a}{RT}-\frac{1}{2}\right)\frac{\alpha\mathrm{Kn}}{1+\alpha\mathrm{Kn}} \quad (41)$$

The pair of Eqs. (32) and (41) thus uniquely determine the optimum pressure and temperature.

In general, Eqs. (32) and (41) must be solved as a coupled pair to obtain the optimum pressure and temperature. Surprisingly this is not the case here. Equation (41) alone can be simplified to yield a relation between the optimum temperature and the optimum Knudsen number.

$$\frac{E_a}{RT}=\frac{1}{2\alpha\mathrm{Kn}}=\frac{\pi w N\sigma^2 p}{\sqrt{2}\,\alpha RT} \quad (42)$$

Eliminating the temperature from this result gives an explicit expression for the optimum pressure.

$$p=\frac{\sqrt{2}\,\alpha E_a}{\pi w N\sigma^2} \quad (43)$$

This is a remarkable result in that the optimum pressure does not depend on the process temperature, the prescribed uniformity, nor on the wafer size. It depends only on the activation energy for the deposition reaction, the composition of the gas mixture, species properties of the mixture gases, and the size of the inter-wafer space.

To solve for the optimum temperature and to plot resulting deposition rates, it is useful to rewrite the uniformity condition, Eq. (32), in terms of normalized variables. For this purpose, the normalized pressure, temperature and density are defined as $p^*=p/p_{\mathrm{R}}$, $T^*=T/T_{\mathrm{R}}$, and $\rho^*=\rho/\rho_{\mathrm{R}}$. Similarly, the normalized deposition rate and molecular speed are $S^*=S/S_{\mathrm{R}}$ and $\overline{v}^*=\overline{v}/\overline{v}_{\mathrm{R}}$. The reference temperature, density

and speed for this first-order deposition reaction are taken as

$$T_{\mathrm{R}} = \frac{E_a}{R} \quad \rho_{\mathrm{R}} = \frac{1}{\sqrt{2}\,\pi w N \sigma^2} \quad \overline{v}_{\mathrm{R}} = \left(\frac{8RT_{\mathrm{R}}}{\pi m}\right)^{1/2} \quad (44)$$

We additionally require that the reference density, pressure and temperature satisfy the ideal gas equation of state, $p_{\mathrm{R}} = \rho_{\mathrm{R}} R T_{\mathrm{R}}$. The normalized density and normalized molecular speed follow directly from these relations.

$$\rho^* = \frac{p^*}{T^*} = \frac{1}{\mathrm{Kn}} \quad \text{and} \quad \bar{v}^* = \sqrt{T^*} \qquad (45a,b)$$

Under this scaling the optimum pressure given by Eq. (43) is $p^* = 2\alpha$.

Now taking $S_{\mathrm{R}} = b\,\overline{v}_{\mathrm{R}}\rho_{\mathrm{R}}/4$ as the reference deposition rate, the normalized deposition rate may be written as

$$S^* = \bar{v}^* \rho^* f_a\, e^{-1/T^*} = \frac{p^*}{\sqrt{T^*}} f_a\, e^{-1/T^*} \qquad (46)$$

Finally, for this first-order deposition reaction the deposition modulus, defined by Eqs. (11) and (17), may be written as

$$\beta_a = \frac{2Sa^2}{\rho D w f_a} = \frac{\overline{v}}{2}\frac{a^2}{w}\frac{\phi}{D} \qquad (47a,b)$$

$$= \frac{3b}{2}\left(\frac{a}{w}\right)^2 \left(\frac{1+\alpha \mathrm{Kn}}{\alpha \mathrm{Kn}}\right) e^{-1/T^*} \qquad (47c)$$

Substituting this expression into Eq. (32), setting the pressure to the optimum value $p^* = 2\alpha$, and rearranging slightly gives the desired expression for the optimum temperature,

$$U^* \equiv \frac{8}{3b}\left(\frac{w}{a}\right)^2 (1-U) \qquad (48a)$$

$$= \left(1+\psi f_a\right)\left(1+\frac{p^*}{\alpha T^*}\right) e^{-1/T^*} \qquad (48b)$$

$$= \left(1+\psi f_a\right)\left(1+\frac{2}{T^*}\right) e^{-1/T^*} \qquad (48c)$$

where U^* is referred to here as the normalized nonuniformity. It is defined by Eq. (48a) such that the uniformity is fixed whenever U^* is fixed for a given wafer size and wafer spacing.

The transcendental equation (48c) defining the optimum temperature can be solved easily by means of successive substitution. Beginning with the initial approximation of $1/T^* = -\ln U^*$, this procedure usually converges in just a few cycles for all values of U^* of practical importance.

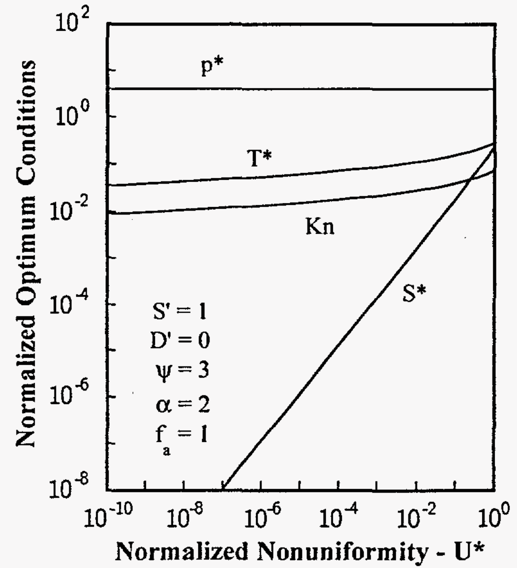

Figure 4. Normalized optimum conditions as a function of normalized nonuniformity. Increasing nonuniformity permits higher processing temperatures and higher deposition rates.

Sample calculations of the optimum normalized pressure, temperature and deposition rate, as well as the optimum Knudsen number, are shown in Fig. 4 as a function of the normalized nonuniformity U^*. As noted above the optimum pressure is independent of U^* and is given by $p^* = 2\alpha = 4$ for the sample conditions shown. Due to the Arrhenius temperature dependence of the deposition rate, the optimum normalized temperature varies weakly with nonuniformity. It increases by only a factor of six as the nonuniformity varies by 10 orders of magnitude. Because the pressure is fixed, the Knudsen number at the optimum conditions shows a similarly weak dependence on the uniformity. Despite these weak variations in the optimum conditions, the maximum normalized deposition rate exhibits a nearly linear increase with increasing nonuniformity. The reason for this is that the normalized temperature is small over the range of conditions shown. In this limit of $T^* \to 0$, the normalized deposition rate can be written as $S^* \approx \alpha\sqrt{T^*}U^* f_a/(1+\psi f_a)$. Thus the maximum deposition rate differs by less than a factor of three from a linear dependence on the nonuniformity as the nonuniformity varies from 10^{-10} to 10^0.

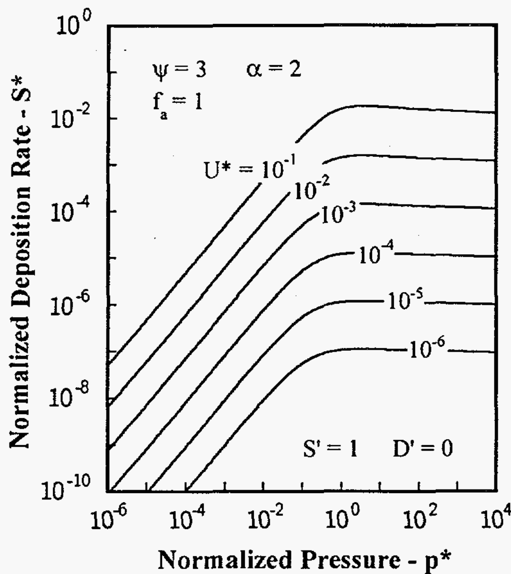

Figure 5. Normalized deposition rates near the optimum pressure. Deposition rates exhibit a weak one-sided maximum with the deposition rate falling very slowly at pressures above the optimum.

Although Eqs. (43) and (48) define optimum conditions giving the maximum deposition rate at fixed uniformity, they provide no insight into the character of this maximum. To gain this insight, we need to examine the variation of the deposition rate in the vicinity of the optimum conditions following a path of constant uniformity. This is depicted in Fig. 5. Here the normalized deposition rate is shown as a function of the normalized pressure, for fixed values of the normalized nonuniformity. At each pressure along each curve the corresponding temperature is computed using Eq. (48b) and the specified nonuniformity. The normalized deposition rate is then computed from Eq. (46). Using this approach the uniformity constraint is always satisfied, even though the pressure and temperature are not necessarily optimum.

We see in Fig. 5 that the deposition rate exhibits a weak one-sided maximum; at all pressures above the optimum value, the deposition rate is nearly constant. It is very important to note that this behavior is not peculiar to the first-order deposition reaction given by Eq. (38). Any transport and deposition process adequately described by the general form of Eqs. (1) and (2), regardless of details of the deposition mechanism, will give a deposition rate at fixed uniformity that is nearly constant at high pressure and that falls linearly with pressure as the pressure is reduced below the optimum value.

Discussion of Low Pressure CVD

As described above deposition rates at fixed uniformity are insensitive to pressure at high pressures, but vary strongly with pressure when pressures are very low. The reason for this becomes apparent when Eqs. (11) and (32) are combined in their dimensional form. This combination yields

$$\mathrm{S}'(1+\psi f_a)\, a^2 S = 2\,(1-U)\,\rho\, D\, w f_a \qquad (49)$$

Thus for fixed geometry, a fixed reactant mole fraction, any fixed order of the deposition reaction and fixed net reaction yield, the surface deposition rate is proportional to the triple product of the nonuniformity, density and diffusivity. At high pressures, where ordinary diffusion is dominant, the product ρD exhibits no first-order pressure dependence, so the deposition rate must remain nearly constant when the uniformity is fixed. At low pressures, where Knudsen diffusion is dominant, the diffusivity exhibits no pressure dependence and so the product ρD falls linearly with pressure. In this case, the deposition rate must similarly fall in proportion to the pressure if the uniformity is to remain constant. As such, increased uniformity usually can be obtained only at the expense of reduced surface deposition rate. The only exception to this is when the order of the deposition reaction falls with decreasing pressure, and such behavior is unusual. In most cases, the order of a surface reaction falls with increasing pressure due to surface saturation and to the increasing importance of reverse reactions. Again, these conclusions do not depend in any way on details of the deposition reaction, but instead require only that the nonuniformity is small and that the transport and deposition process can be described by the form of Eqs. (1) and (2).

These observations contradict the conventional view that low pressures lead to increased uniformity due to the increase in diffusivity. The origin of that view seems to lie in the misleading form of Eq. (47b), showing that the deposition modulus, and so the nonuniformity, is inversely proportional to the diffusivity. Indeed the diffusivity contains the only pressure dependence in this expression. However, from Eqs. (11) and (32) we see that in general $U^* \propto \beta_a \propto S/\rho D$. Thus in the regime of ordinary diffusion, where the product ρD is nearly constant, the uniformity will vary linearly with pressure for a first-order deposition reaction, but will vary as the square of the pressure for a second-order process. In general, for ordinary diffusion the pressure dependence of the uniformity will be the same as the pressure dependence of the deposition rate. We therefore conclude that the variation of uniformity with pressure arises not from variation in

the diffusivity, but instead arises from variation in the deposition rate. Equations (47b) and (47c) are simply misleading because the linear pressure dependence of the first-order surface deposition reaction is confused with the linear pressure dependence of the diffusivity.

The preceding conclusions leave little motivation for using low-pressure CVD processes. We have shown that high deposition rates and high uniformity can both be obtained at arbitrarily high pressures and that the only means to increase uniformity is to reduce the deposition rate. This can be accomplished either by reducing the pressure at a fixed temperature, as often practiced, or by reducing the temperature at a fixed pressure. These are equivalent in terms of reducing the deposition rate and increasing the uniformity. However, because low temperatures are more easily obtained than are low pressures, some additional concern must underlie the widespread use and success of low-pressure CVD in batch furnaces.

Optimum Conditions at Fixed Uniformity and Fixed Relative Nucleation Rate

From the results so far we see that deposition uniformity alone is not sufficient motivation to perform CVD processes at low pressures and that some addition constraint must motivate this practice. In some cases the process temperature is fixed by a requirement on the morphology of the deposited layer. In others, complex gas-phase chemistries may dictate a preferred operating condition. Here we will consider yet another requirement, that particle formation in the gas phase is not excessive. Such particles may be deposited on the wafer surfaces, leading to unacceptable device performance.

To address this concern, we first define the relative nucleation rate as the ratio of the particle generation rate in the volume between wafers to the total surface deposition rate on the two wafer faces. This can be written as

$$\Omega = \frac{w}{2}\frac{H}{S} \tag{50}$$

where H is the homogeneous particle nucleation rate, and Ω is referred to as the relative nucleation rate.

When deposition uniformity alone constrains the deposition rate, the deposition rate can be increased by increasing the reactant mole fraction. Since increasing the reactant fraction also encourages particle nucleation, the constrained maximum deposition rate should occur when both the uniformity constraint and nucleation constraint are just marginally satisfied. As before, this permits replacing the inequality constraint that the uniformity should be better than some value by an equality constraint that is satisfied exactly. Likewise, the inequality constraint that the relative nucleation rate is smaller than some value can be replaced by a specification on the relative nucleation rate.

As in the case of fixed uniformity alone, we use the method of Lagrange multipliers to identify the optimum conditions maximizing deposition rate when both the uniformity and the relative gas-phase nucleation rate are specified at acceptable levels. Again this approach yields one new unknown for each constraint and one new equation for each independent variable. The three new equations are

$$\frac{\partial S}{\partial p} - \kappa_1\frac{\partial U}{\partial p} - \kappa_2\frac{\partial \Omega}{\partial p} = 0 \tag{51}$$

$$\frac{\partial S}{\partial T} - \kappa_1\frac{\partial U}{\partial T} - \kappa_2\frac{\partial \Omega}{\partial T} = 0 \tag{52}$$

$$\frac{\partial S}{\partial f_a} - \kappa_1\frac{\partial U}{\partial f_a} - \kappa_2\frac{\partial \Omega}{\partial f_a} = 0 \tag{53}$$

and the two new unknown constants are the Lagrange multipliers κ_1 and κ_2. The three independent variables in this case are the pressure, temperature and reactant mole fraction.

Eliminating the Lagrange multipliers from these three equations gives

$$\frac{\partial S}{\partial T}\left(\frac{\partial U}{\partial p}\frac{\partial \Omega}{\partial f_a} - \frac{\partial U}{\partial f_a}\frac{\partial \Omega}{\partial p}\right) - \frac{\partial U}{\partial T}\left(\frac{\partial S}{\partial p}\frac{\partial \Omega}{\partial f_a} - \frac{\partial S}{\partial f_a}\frac{\partial \Omega}{\partial p}\right) - \frac{\partial \Omega}{\partial T}\left(\frac{\partial S}{\partial f_a}\frac{\partial U}{\partial p} - \frac{\partial S}{\partial p}\frac{\partial U}{\partial f_a}\right) = 0 \tag{54}$$

Rearranging this expression to collect together those terms multiplied by derivatives of the uniformity, and expanding those derivatives using the first-order term of Eq. (32) yields

$$\left(\frac{1}{\mathbf{S}'}\frac{\partial \mathbf{S}'}{\partial p} - \frac{1}{\rho}\frac{\partial \rho}{\partial p} - \frac{1}{D}\frac{\partial D}{\partial p}\right)\left(\frac{\partial S}{\partial T}\frac{\partial \Omega}{\partial f_a} - \frac{\partial S}{\partial f_a}\frac{\partial \Omega}{\partial T}\right) - \left(\frac{1}{\mathbf{S}'}\frac{\partial \mathbf{S}'}{\partial T} - \frac{1}{\rho}\frac{\partial \rho}{\partial T} - \frac{1}{D}\frac{\partial D}{\partial T}\right)\left(\frac{\partial S}{\partial p}\frac{\partial \Omega}{\partial f_a} - \frac{\partial S}{\partial f_a}\frac{\partial \Omega}{\partial p}\right) - \left(\frac{1}{\mathbf{S}'}\frac{\partial \mathbf{S}'}{\partial f_a} - \mathbf{D}' + \frac{\psi}{1+\psi f_a} - \frac{1}{f_a}\right) \times \left(\frac{\partial S}{\partial T}\frac{\partial \Omega}{\partial p} - \frac{\partial S}{\partial p}\frac{\partial \Omega}{\partial T}\right) = 0 \tag{55}$$

Derivatives useful in obtaining this result are given in Appendix B. This relation, the uniformity constraint given by Eq. (32), and the nucleation constraint given

by Eq. (50) form a system of three nonlinear equations that can be solved for the optimum process conditions. Again these equations are quite general, requiring only that the problem is well described by Eqs. (1) and (2) and that the deposition nonuniformity is small.

Sample Calculations - Fixed Uniformity and Fixed Relative Nucleation Rate

The supersaturation in CVD processes is often very large [1,21]. In this limit, the critical cluster size for stable particle formation is on the order of a single atom and classical theory of homogeneous nucleation does not apply [22]. Instead, the particle nucleation rate can be described in part by an irreversible second-order reaction [21,23],

$$H = \frac{\pi}{\sqrt{2}} N\sigma^2 \bar{v} (\rho f_a)^2 \phi' \tag{56}$$

where H is the homogeneous dimer nucleation rate, and the reaction probability for gas-phase collisions is

$$\phi' = b' e^{-E_a'/RT} \tag{57}$$

All other variables appearing above are the same as previously defined for the first-order surface deposition reaction.

We note that Eq. (56) describes only an initial step in particle formation. In order to form macroscopic solids, clusters of a few atoms must subsequently grow by continued deposition from the gas phase or by cluster coagulation. However, since we are interested here only in a qualitative indication of the tendency for particle formation, this initial step provides a satisfactory description of the nucleation process for purposes of constraining the optimization of deposition rate.

Using the first-order surface deposition rate given by Eq. (38), the relative nucleation rate may be written as

$$\Omega = \sqrt{2}\pi w N\sigma^2 \rho f_a \frac{\phi'}{\phi} \tag{58}$$

where, as before, ϕ is the reaction probability for the surface reaction. Noting that the product $\sqrt{2}\pi N\sigma^2\rho$ is the inverse of the mean free path, Eq. (58) may be rewritten as

$$\Omega = \frac{f_a}{\mathrm{Kn}} \frac{\phi'}{\phi} = \frac{f_a}{\mathrm{Kn}} \frac{b'}{b} e^{-\epsilon E_a/RT} \tag{59}$$

where again, $\mathrm{Kn} = \lambda/w$ is the Knudsen number. The parameter

$$\epsilon = \frac{E_a'}{E_a} - 1 \tag{60}$$

indicates the relative magnitude of the activation energies for the nucleation and deposition reactions.

Based on this first-order deposition reaction and second-order nucleation reaction, the deposition rate and relative nucleation rate each satisfy

$$\frac{1}{S}\frac{\partial S}{\partial p} = \frac{1}{\Omega}\frac{\partial \Omega}{\partial p} = \frac{1}{p} \qquad \frac{1}{S}\frac{\partial S}{\partial f_a} = \frac{1}{\Omega}\frac{\partial \Omega}{\partial f_a} = \frac{1}{f_a} \tag{61}$$

Dividing Eq. (55) by the product $S\,\Omega$ and substituting the expressions above into the result gives

$$\left(\frac{1}{S}\frac{\partial S}{\partial T} - \frac{1}{\Omega}\frac{\partial \Omega}{\partial T}\right)\left[\frac{1}{f_a}\left(\frac{1}{\rho}\frac{\partial \rho}{\partial p} + \frac{1}{D}\frac{\partial D}{\partial p}\right) + \frac{1}{p}\left(\frac{\psi}{1+\psi f_a} - \mathbf{D}' - \frac{1}{f_a}\right)\right] = 0 \tag{62}$$

This equation yields two possible roots for the optimum conditions. The leading term (in parentheses) vanishes when the derivative of the log of the nucleation rate, H, is twice that of deposition rate, S. However, this root yields a local minimum of the deposition rate at the condition $E_a/RT = 2(\epsilon - 1)$. The conditions yielding the maximum must therefore arise from a zero of the second term (in brackets). Taking this into account and using the diffusivity based on kinetic theory and the normalized ideal gas relation, Eq. (62) may be written as

$$\frac{\psi f_a}{1+\psi f_a} = \frac{1}{1+\alpha \mathrm{Kn}}\left(1 + \frac{f_a}{\alpha}\frac{\partial \alpha}{\partial f_a}\right) \tag{63}$$

This result, the uniformity constraint given by Eq. (32), and the nucleation constraint given by Eq. (58) are the three equations defining the optimum pressure, temperature and reactant mole fraction. As before, these must be solved as a coupled system to obtain the optimum process conditions.

Equation (63) can be simplified further by assuming that the derivative of the diffusivity with respect to the reactant mole fraction is negligible. For a simple binary mixture of the reactant and a single diluent gas, $\partial\alpha/\partial f_a$ is exactly zero due to the reciprocity condition that binary diffusivities must satisfy. Further, the effective binary diffusivity of the reactant and a gas mixture also shows no dependence on the reactant fraction provided that the composition of the mixture does not vary with the reactant fraction. This

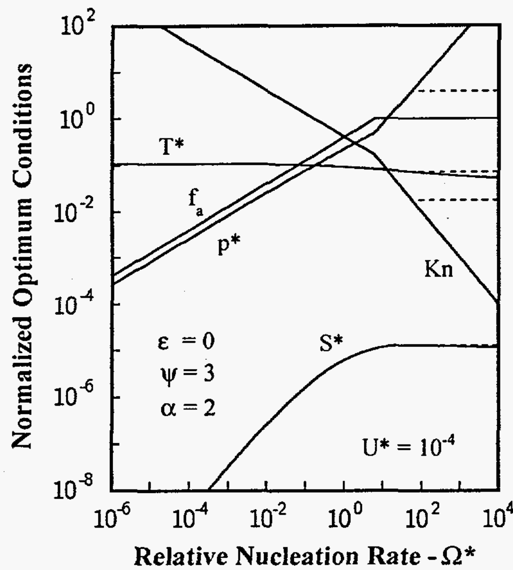

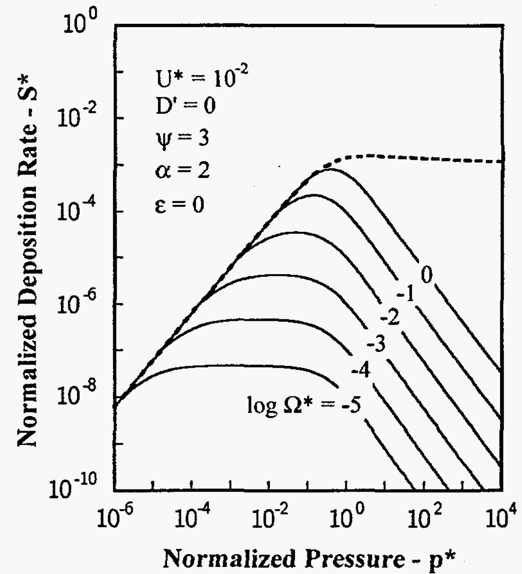

Figure 6. Optimum conditions for fixed uniformity and fixed relative nucleation rate. Dashed curves show regions of higher deposition rate at nucleation rates below the required value.

Figure 7. Normalized deposition rates near the optimum pressure for fixed uniformity and fixed normalized nucleation rate. Deposition rates exhibit a strong maximum.

assumption should therefore remain valid for many practical process conditions, and Eq. (63) yields

$$\psi f_a = \frac{1}{\alpha \mathrm{Kn}} \tag{64}$$

relating the optimum reactant fraction to the optimum Knudsen number.

To plot optimum conditions for this sample problem, it is again useful to normalize the dependent and independent variables using Eqs. (44) through (48). We also introduce one new parameter,

$$\Omega^* \equiv \Omega \frac{b}{b'} = \frac{f_a}{\mathrm{Kn}} e^{-\epsilon/T^*} = f_a \frac{p^*}{T^*} e^{-\epsilon/T^*} \tag{65}$$

referred to here as the normalized relative nucleation rate. Combining this definition with the normalized uniformity constraint given by Eq. (48a) and the optimum given by Eq. (64) then yields

$$\left(1 + \psi f_a\right)^2 e^{-1/T^*} = U^* \tag{66}$$

and

$$\alpha \psi f_a^2 \, e^{-\epsilon/T^*} = \Omega^* \tag{67}$$

For specified values of α, ψ and ϵ, this pair of equations can be solved for the optimum temperature and reactant mole fraction. The corresponding value of the optimum pressure can then be computed from Eq. (64).

Sample calculations of the optimum conditions at fixed uniformity and fixed allowable nucleation rate are shown in Fig. 6. We see that the pressure and reactant fraction both increase roughly as the square-root of the normalized nucleation rate, while the optimum temperature varies little as the nucleation rate increases from 10^{-6} to 10^4. Once the optimum reactant fraction reaches its maximum value of unity, the optimum pressure increases about linearly with increasing nucleation rate while the reactant fraction remains constant.

At sufficiently high values, the relative nucleation rate no longer constrains the optimum conditions, and higher deposition rates can be obtained at less than the maximum allowable nucleation rate. This is shown in Fig. 6 by dashed curves. These are computed using the optimum conditions for a constraint on uniformity only. At each point along these dashed curves, the deposition rate exceeds that of the doubly constrained maximum (though only slightly) and the normalized relative nucleation rate is smaller than the value indicated on the axis of the plot.

As in the previous sample calculations, these optimum conditions provide no information concerning the character of the maximum. We therefore need to examine again the variation of the deposition rate in the vicinity of the optimum conditions, following in this case a path of both constant uniformity and con-

stant relative nucleation rate. This is illustrated in Fig. 7, where the normalized deposition rate is shown as a function of pressure for a single value of the normalized nonuniformity and a range of values of the relative nucleation rate. The curves in this figure are computed by specifying the pressure and then solving Eqs. (48a) and (65) together to obtain the temperature and reactant mole fraction. By this method both constraints are satisfied along each curve, even though the conditions are not necessarily optimum. The dashed curve in Fig. 7 is the deposition rate constrained only by a uniformity condition. This previously appeared in Fig. 5. Note that the additional constraint on the nucleation rate always reduces the optimum pressure.

In Fig. 7 we see that dual constraints on the uniformity and relative nucleation rate yield a strong maximum in the normalized deposition rate. In contrast with Fig. 5, the deposition rate here falls about linearly both above and below the optimum pressure. As the nucleation constraint becomes increasingly stringent, $\Omega^* \to 0$, a plateau develops about the maximum, but outside this plateau the deposition rate still falls sharply. From this we see that low-pressure CVD offers a distinct advantage over ambient pressure processing when both uniformity and gas-phase particle nucleation are considered.

Finally, the system of equations (64), (66) and (67) can be solved in closed form for the special case of $f_a \ll 1$. In this limit, corresponding to a very stringent requirement on the nucleation rate, the optimum reactant mole fraction and normalized temperature are

$$f_a = \left(\frac{\Omega^*}{\alpha\psi U^{*\epsilon}}\right)^{1/2} \quad \text{and} \quad T^* = -\frac{1}{\ln U^*} \qquad (68a, b)$$

The optimum pressure for this special case then follows directly from Eq. (64),

$$p^* = \alpha\psi f_a T^* = -\frac{1}{\ln U^*}\left(\frac{\alpha\psi\Omega^*}{U^{*\epsilon}}\right)^{1/2} \qquad (69)$$

and by Eq. (46) the normalized deposition rate at the optimum conditions is

$$S^* = \frac{\Omega^* U^{*1-\epsilon}}{\sqrt{-\ln U^*}} \qquad (70)$$

Thus the deposition rate at the optimum conditions is proportional to the relative particle nucleation rate, and increasingly stringent requirements on particle nucleation rates must be paid for with decreased deposition rate and increased processing time.

Application to CVI

Chemical vapor infiltration (CVI), used to coat and densify porous preforms for manufacturing high-performance composites, is completely analogous to the CVD process. As such, the results obtained here can be applied to that problem by making a few simple substitutions: (1) any appearance of the inter-wafer space, w, by itself is replaced by the characteristic pore size, d; (2) the group a^2/w is replaced by $s_v a^2/2$, where s_v is the specific surface area of the porous material; and the group $(a/w)^2$ is replaced by $s_v a^2/2d$. Additionally, the diffusivity ratio, α, is replaced everywhere by the product αD^*, where D^* is the dimensionless effective diffusivity of the preform. Using these substitutions, the optimum pressure, temperature and reactant mole fraction can be computed for CVI processes performed on cylindrical preforms. All results based on the first-order perturbation solution may also be applied to rectangular geometries simply by dividing the diffusivity ratio, α, by two.

Summary

Deposition rates for CVD processes performed in multi-wafer batch furnaces are generally limited by the requirement of high radial uniformity of the deposited layer and by stringent requirements on gas-phase particle generation. To obtain high deposition rate and corresponding high furnace throughput, CVD process recipes must be carefully optimized.

To help optimize CVD process conditions, we have derived an analytical expression relating deposition uniformity to the surface deposition rate. This expression is based on a perturbation solution describing the radial advective and diffusive transport and surface deposition of a single reactive species. The analysis accounts for both ordinary and Knudsen diffusion and is applicable to any deposition reaction, provided that the deposition nonuniformity is small.

Based on the first-order perturbation solution, the deposition rate is first maximized subject to a constraint on the radial uniformity of the deposition rate. Both optimum pressure and optimum temperature are determined by the method of Lagrange multipliers. Sample calculations for the special case of a first-order deposition reaction show that the optimum pressure depends on the activation energy for the deposition reaction, the size of the inter-wafer space, the composition of the gas mixture, and on properties of all species in the mixture. Surprisingly, it does not depend on the prescribed uniformity or on the wafer diameter. In contrast, the optimum temperature depends on the prescribed uniformity, pre-exponential constant and the activation energy, as well as the net

molar yield of the deposition reaction and the ratio of the inter-wafer space to the wafer radius. The optimum temperature does not depend on the composition of the furnace gas or on properties of the mixture species.

The optimum conditions for a given uniformity yield a weak one-sided maximum of the deposition rate. The deposition rate falls sharply at pressures below the optimum value, but remains nearly constant at all pressures above. The reason for this latter behavior is that the nonuniformity is proportional to the ratio of the deposition rate and the product of the gas density and diffusivity. Because the product of the density and diffusivity exhibits no first-order pressure dependence when Knudsen diffusion is unimportant, the deposition rate must be nearly constant whenever the uniformity is fixed. Further, the pressure dependence of the uniformity and of the deposition rate are the same for any deposition reaction of fixed order in the reactant fraction.

Contrary to the conventional view, uniformity does not increase with decreasing pressure because of the increase in diffusivity. Although diffusivities do indeed increase with decreasing pressure, this increase in diffusivity is just offset by a decrease in gas density such that diffusive fluxes are independent of pressure when ordinary diffusion is dominant. Rather, uniformity increases with decreasing pressure only if the deposition rate falls as the pressure is reduced. Because most deposition reactions exhibit at least some pressure dependence, uniformity does generally increase at reduced pressures, but only at the expense of deposition rate.

At sufficiently low pressures, where Knudsen diffusion is dominant, deposition uniformity no longer varies in proportion to the deposition rate. In this limit, the diffusivity is independent of pressure, and diffusive fluxes are therefore proportional to the pressure. Here the pressure dependence of the deposition rate must exceed a linear dependence if the uniformity is to increase as the pressure is further reduced.

Since high deposition rates and high uniformity can both be obtained at high pressures, some additional constraint must motivate the use of low-pressure processes. Although several concerns may provide this motivation, we have examined here only the issue of gas-phase particle nucleation. The method of Lagrange multipliers is again employed to maximize the deposition rate, subject in this case to constraints on both radial uniformity and a relative rate of gas-phase nucleation. Sample calculations for a first-order deposition reaction and second-order nucleation process indicate that both the optimum pressure and the optimum reactant fraction should be roughly proportional to the square root of the relative nucleation rate. In this case, the deposition rate exhibits a strong maximum, with rates falling steeply both above and below the optimum pressure. Reduced pressures may therefore permit large increases in the deposition rate for deposition reactions prone to gas-phase particle generation.

Nomenclature

a	wafer radius
b	reaction pre-exponential constant
D	effective binary diffusivity
D_m	effective ordinary binary diffusivity
D_{Kn}	reactant Knudsen diffusivity $(D_{\mathrm{Kn}} = \overline{v}w/3)$
$\mathbf{D}'$	order of diffusivity in reactant fraction
E_a	reaction activation energy
f	reactive species mole fraction
G	uniformity function
H	homogeneous nucleation rate
Kn	Knudsen number $(\mathrm{Kn} = \lambda/w)$
m	reactive species molecular weight
N	Avogadro number
p	total gas pressure
r	radial position
R	ideal gas constant
S	surface deposition rate
$\mathbf{S}'$	order of deposition reaction in reactant fraction
T	temperature
u	radial fluid speed
U	deposition uniformity
$\overline{v}$	reactant mean molecular speed
w	inter-wafer space
x	normalized radial position $(x = r/a)$
α	ratio of self to mixture diffusivities
β_a	surface deposition modulus
λ	reactant mean free path
κ	Lagrange multiplier
ρ	total molar density
σ	reactive species molecular diameter
ϕ	reaction probability
ψ	net molar yield of deposition reaction
Ω	relative homogeneous nucleation rate

Subscripts and Superscripts

a	at wafer edge
i	order of perturbation solution
R	reference value for normalization
$'$	prime denotes homogeneous nucleation reaction
$*$	asterisk denotes normalized variable

Acknowledgment

The authors wish to thank Dr. R. S. Larson for his very careful review of this paper and Dr. R. W. Foote for sharing with us his broad experience in wafer processing. This work was funded in part by a Sandia National Laboratories Cooperative Research and Development Agreement (CRADA) with SEMATECH, in part by the Advanced Research Projects Agency (ARPA) High Temperature Structural Materials Program, and in part by the US Department of Energy Office of Industrial Technologies, Advanced Industrial Materials Program.

References

1. D. W. Hess and K. F. Jensen, **Microelectronics Processing**, p. 1, Advances in Chemistry, Series 221, American Chemical Society, Washington, DC (1989).

2. A. Sherman, **Chemical Vapor Deposition For Microelectronics**, p. 1, Noyes Publications, Park Ridge, NJ (1987).

3. T. A. Badgwell, T. F. Edgar and I. Trachtenberg, "Modeling and Scale-Up of Multiwafer LPCVD Reactors," *AIChE J.*, **38**, 926 (1992).

4. L. M. Zambov, "Optimum Design of LPCVD Reactors," *J. de Physique IV,* Colloque C, **5**, 269 (1995).

5. S. Wolf and R. N. Tauber, **Silicon Processing for the VLSI Era,** p. 170, Lattice Press, Sunset Beach, CA (1986).

6. G. B. Raupp, D. A. Levedakis and T. S. Cale, "Predicting Interwafer Film Thickness Uniformity in an Ultralow Pressure Chemical Vapor Deposition Reactor," *J. Vac. Sci. Technol.,* **A11**, 3053 (1993).

7. C. Galewski and W. G. Oldham, "Modeling of a High Throughput Hot-Wall Reactor for Selective Epitaxial Growth of Silicon," *IEEE Trans. Semicond. Manufact.*, **5**, 169 (1992).

8. K. F. Jensen and D. B. Graves, "Modeling and Analysis of Low Pressure CVD Reactors," *J. Electrochem. Soc.: Solid-State Sci. and Technol.,* **130**, 1950 (1983).

9. Z. M. Qian, H. Michiel, A. Van Ammel, J. Nijs and R. Mertens, "Homogeneous Gas Phase Nucleation of Silane in Low Pressure Chemical Vapor Deposition (LPCVD)," *J. Electrochem. Soc.: Solid-State Sci. and Technol.,* **135**, 2378 (1988).

10. K. Okuyama, D. D. Huang, J. H. Seinfeld, N. Tani and I. Matsui, "Gas-Phase Nucleation in GaAs Thin Film Preparation by Metal Organic Chemical Vapor Deposition," *Jpn. J. Appl. Phys.,* **31**, Part 1, 1 (1992).

11. M. Adachi, K. Okuyama, N. Tohge, M. Shimada, J. Satoh and M. Muroyama, "Gas-Phase Nucleation in an Atmospheric Pressure Chemical Vapor Deposition Process for SIO_2 Films Using Tetraethylorthosilicate (TEOS)," *Jpn. J. Appl. Phys.,* **31**, Part 2, 1439 (1992).

12. W. A. Brown and T. I. Kamis, "An Analysis of LPCVD System Parameters for Polysilicon, Silicon Nitride and Silicon Dioxide Deposition," *Solid State Technology,* July 1979.

13. B. Gelernt, "Selecting an Organosilicon Source for LPCVD Oxide," *Semiconductor International,* March 1990.

14. W. G. Houf, J. F. Grcar and W. G. Breiland, "A Model for Low Pressure Chemical Vapor Deposition in a Hot-Wall Tubular Reactor," *Mater. Sci. and Eng.,* **B17**, 163 (1993).

15. M. E. Coltrin, R. J. Kee and J. A. Miller, "A Mathematical Model of Silicon Chemical Vapor Deposition," *J. Electrochem. Soc.: Solid-State Sci. and Technol.,* **133**, 1206 (1986).

16. G. D. Papasouliotis and S. V. Sotirchos, "On the Homogeneous Chemistry of the Thermal Decomposition of Methyltrichlorosilane," *J. Electrochem. Soc.: Solid-State Sci. and Technol.,* **141**, 1599 (1994).

17. C. Bonsanquet, British T. A. Report, BR 507 (1944). See also W. G. Pollard and R. D. Present, *Phys. Rev.,* **73**, 762 (1948).

18. J. O. Hirschfelder, C. F. Curtiss and R. B. Bird, **Molecular Theory of Gases and Liquids**, p. 13, John Wiley & Sons, New York, NY (1954).

19. W. E. Stewart and J. V. Villadsen, "Graphical Calculation of Multiple Steady States and Effectiveness Factors for Porous Catalysts," *AIChE J.,* **15**, 28 (1969).

20. W. Kaplan, **Advanced Calculus**, p. 184, Addison-Wesley, Reading, MS (1973).

21. K. Okuyama, D. Huang, J. H. Seinfeld, N. Tani and Y. Kousaka, "Aerosol Formation by Rapid Nucleation During the Preparation of SiO_2 Thin Films from $SiCl_4$ and O_2 Gases by CVD Processes," *Chem. Eng. Sci.,* **46**, 1545 (1991).

22. G. S. Springer, "Homogeneous Nucleation," *Advances in Heat Transfer,* **14**, 281 (1978).

23. F. Wilkinson, **Chemical Kinetics and Reaction Mechanisms**, p. 105, Van Nostrand Reinhold Company, New York, NY (1980).

24. R. B. Bird, W. E. Stewart and E. M. Lightfoot, **Transport Phenomena**, p. 571, John Wiley & Sons, New York, NY (1960).

Appendix A

The parameter α is the ratio of the effective binary coefficient of ordinary diffusion for the reactive species and the mixture of other furnace gases to the coefficient of ordinary self diffusion for the reactive species. Denoting the coefficient for the mixture as D_{1m} and the coefficient for the reactive species only as D_{11}, this may be written

$$\alpha = \frac{D_{1m}}{D_{11}} \tag{A1}$$

The values of the terms on the right of Eq. (A1) may be computed by any number of methods, ranging from the very simple to very complete. Here we consider a very simple method based on kinetic theory and the rigid sphere approximation.

The effective binary coefficient of ordinary diffusion for the reactive species in a gas mixture may be expressed as [24]

$$\frac{1 - x_1}{D_{1m}} = \sum_{j=2}^{n} \frac{x_j}{D_{1j}} \tag{A2}$$

where x_j are the mole fractions of each species, and D_{1j} is the binary coefficient of ordinary diffusion for the reactive species paired with species j. In this case the subscript $j = 1$ refers to the species of interest, while $j = 2$ and above refer to all other species in the mixture. Combining Eqs. (A1) and (A2) yields an expression for α in terms of the binary coefficients of diffusion only.

$$\frac{1}{\alpha} = \frac{1}{1 - x_1} \sum_{j=2}^{n} x_j \frac{D_{11}}{D_{1j}} \tag{A3}$$

Now assuming the hard sphere molecular behavior, the ratio D_{11}/D_{1j} may be written as

$$\frac{D_{11}}{D_{1j}} = \left(\frac{\sigma_1 + \sigma_j}{2\sigma_1}\right)^2 \left(\frac{2m_j}{m_1 + m_j}\right)^{1/2} \tag{A4}$$

where σ_j and m_j are the atomic diameter and molecular weight of the jth mixture species. Note that neither the pressure nor temperature appear in this relation because D_{11} and D_{1j} always share the same functional dependence on both. Finally, combining Eqs. (A3) and (A4) gives the desired expression for α.

$$\frac{1}{\alpha} = \frac{1}{1 - x_1} \sum_{j=2}^{n} x_j \left(\frac{\sigma_1 + \sigma_j}{2\sigma_1}\right)^2 \left(\frac{2m_j}{m_1 + m_j}\right)^{1/2} \tag{A5}$$

We now see that the rigid sphere molecular model gives a value for α that depends only the mixture composition and the molecular diameter and weight of all the mixture species. However, a more rigorous treatment based on Chapman-Enskog theory would yield a slight pressure and temperature dependence for the ratio D_{11}/D_{1j}. The value of α in that case would also show a weak dependence on the process conditions for a fixed mixture composition.

We need also keep in mind that the process conditions may directly influence the composition of the furnace gas mixture, so in this sense the diffusivity ratio α will vary with pressure and temperature due to variations in x_j, whether or not the ratios D_{11}/D_{1j} are constant. In this case, the present analysis may be combined with a simple zero or one-dimensional auxiliary model of reactant injection and transport in the annular region outside the wafer stack. Using the specified injection rate and assumed trial values for the optimum pressure and temperature, the results presented here can be used with the auxiliary model to compute the composition of the gas mixture outside the wafer stack. From this estimate of the composition, a value for α and new candidate values for the optimum pressure and temperature can then be calculated. This computational procedure can then be repeated, each time using the final estimates of the optimum conditions as initial guesses for the next iteration. This method should converge quickly because the value of α is a fairly weak function of the composition.

Appendix B

The following derivatives of parameters and variables are useful in deriving optimum processing conditions.

Density:

$$\frac{1}{\rho}\frac{\partial \rho}{\partial p} = \frac{1}{p} \qquad \frac{1}{\rho}\frac{\partial \rho}{\partial T} = -\frac{1}{T} \tag{B1a, b}$$

$$\frac{1}{\rho}\frac{\partial \rho}{\partial f} = 0 \tag{B2}$$

Diffusivity:

$$\frac{1}{D}\frac{\partial D}{\partial p} = -\frac{1}{p}\,\frac{1}{1 + \alpha \mathrm{Kn}} \tag{B3}$$

$$\frac{1}{D}\frac{\partial D}{\partial T} = \frac{1}{T}\left(\frac{1}{1 + \alpha \mathrm{Kn}} + \frac{1}{2}\right) \tag{B4}$$

$$\mathbf{D}' = \frac{1}{D}\frac{\partial D}{\partial f} = -\frac{1}{1 + \alpha \mathrm{Kn}}\,\frac{1}{\alpha}\frac{\partial \alpha}{\partial f} \tag{B5}$$

Uniformity:

$$\frac{1}{1-U}\frac{\partial U}{\partial p} = \frac{1}{D}\frac{\partial D}{\partial p} - \frac{1}{\mathbf{S}'}\frac{\partial \mathbf{S}'}{\partial p} - \frac{1}{S}\frac{\partial S}{\partial p} + \frac{1}{\rho}\frac{\partial \rho}{\partial p} \qquad \text{(B6)}$$

$$\frac{1}{1-U}\frac{\partial U}{\partial T} = \frac{1}{D}\frac{\partial D}{\partial T} - \frac{1}{\mathbf{S}'}\frac{\partial \mathbf{S}'}{\partial T} - \frac{1}{S}\frac{\partial S}{\partial T} + \frac{1}{\rho}\frac{\partial \rho}{\partial T} \qquad \text{(B7)}$$

$$\frac{1}{1-U}\frac{\partial U}{\partial f} = \mathbf{D}' - \mathbf{S}' - \frac{1}{\mathbf{S}'}\frac{\partial \mathbf{S}'}{\partial f} - \frac{\psi}{1+\psi f} + \frac{1}{f} \qquad \text{(B8)}$$

Deposition rate:

$$\frac{1}{S}\frac{\partial S}{\partial p} = \frac{1}{p} \qquad \text{(B9)}$$

$$\frac{1}{S}\frac{\partial S}{\partial T} = \frac{1}{T}\left(\frac{E_a}{RT} - \frac{1}{2}\right) \qquad \text{(B10)}$$

$$\mathbf{S}' = \frac{1}{S}\frac{\partial S}{\partial f} = \frac{1}{f} \qquad \mathbf{S}'' = \frac{1}{S}\frac{\partial^2 S}{\partial f^{*2}} = 0 \qquad \text{(B11}a, b\text{)}$$

Relative nucleation rate:

$$\frac{1}{\Omega}\frac{\partial \Omega}{\partial p} = \frac{1}{p} \qquad \frac{1}{\Omega}\frac{\partial \Omega}{\partial T} = \frac{1}{T}\left(\epsilon\frac{E_a}{RT} - 1\right) \qquad \text{(B12}a, b\text{)}$$

$$\frac{1}{\Omega}\frac{\partial \Omega}{\partial f} = \frac{1}{f} \qquad \text{(B13)}$$

Derivatives of the density and diffusivity follow directly from the ideal gas equation of state and kinetic theory, respectively. Those of the uniformity are general and apply to all forms of the deposition reaction and diffusivity. Derivatives of the deposition rate are specific to a first-order reaction having an Arrhenius temperature dependence. Derivatives of the relative nucleation rate apply only to a first-order deposition reaction and second-order nucleation reaction, each having an Arrhenius temperature dependence. Note that $\mathbf{D}'$, $\mathbf{S}'$ and $\mathbf{S}''$ defined in the text are derivatives with respect to f^*, not f, and are evaluated at $f^* = 1$.

UNLIMITED RELEASE
INITIAL DISTRIBUTION

K. F. Jensen
Massachusetts Institute of Technology
Building 6-469
Chemical Engineering
Cambridge, MA 02139

Sunil Shah
RelMan, Inc.
444 Castro Street, Suite 400
Mountain View, CA 94041

A. Mathur
Honeywell Technology Center
3660 Technology Drive
Minneapolis, MN 55418

SEMATECH
2706 Montopolis Drive
Austin, Tx 78741-6499
Attn: N. Alvi
G. Feit

R. W. Foote
National Semiconductor Corp.
1111 West Bardin Road
Arlington, Tx 76017

C. Sorrell
Office of Advanced Industrial Concepts, EE-232
U.S. Dept. of Energy
1000 Independence Avenue
Washington, D.C. 20585

T. M. Besmann
Oak Ridge National Laboratory
P.O. Box 2008
Oak Ridge, TN 37831-6060

M. Zachariah
National Institue of Standards and Technology
Building 221, Room B312
Gaithersburg, MD 20899

C. B. Shumaker
DuPont Lanxide Composites, Inc.
1300 Marrows Road
P.O. Box 6077
Newark, DE 19714-6077

M. Schrems
IBM East Fishkill
1580 Route 52, Zip 33A
Hopewell Junction, NY 12533

B. Sauter
Wacker Siltronic GmbH
Postfach 11 40
D-84479 Burghausen
Germany

Textron Specialty Materials
2 Industrial Avenue
Lowell, MA 01851
Attn: J. E. Niemoller
R. Suplinskas

0513	R. J. Eagan, 1000
1079	A. D. Romig, 1300
1078	C. W. Gwyn, 1302
0606	P. Esherick, 1311
0710	G. A. Carlson, 6211
9001	T. O. Hunter, 8000
	Attn: M. E. John, 8100
	A. West, 8200
	R. C. Wayne, 8400
	A. West, 8600
	T. M. Dyer, 8700
	L. E. Hiles, 8800
	D. L. Crawford, 8900
9403	J. M. Hruby, 8230
9054	W. J. McLean, 8300
	Attn: C. W. Robinson, 8301
	W. Bauer, 8302
	L. A. Rahn, 8351
	F. P. Tully, 8353
	G. A. Fisk, 8355
	R. W. Carling, 8362
9042	R. J. Kee, 8303
9042	G. H. Evans, 8345
9042	J. F. Grcar, 8345
9042	S. K. Griffiths, 8345 (10)
9042	C. M. Hartwig, 8345
9042	W. G. Houf, 8345
9042	R. S. Larson, 8345
9042	E. Meeks, 8345
9042	C. D. Moen, 8345
9042	R. H. Nilson, 8345 (10)
9042	P. A. Spence, 8345
9052	M. D. Allendorf, 8361 (5)
9052	D. R. Hardesty, 8361
9053	S. R. Vosen, 8362
0834	W. L. Hermina, 9111
9021	Technical Communications, 8535 for OSTI (10)
9021	Technical Communications, 8535
8099	Technical Library, 13414 (4)
9018	Central Technical Files, 8523-2 (3)